

Supplementary Information: High Spin-Wave Propagation Length Consistent with Low Damping in a Metallic Ferromagnet

Luis Flacke,^{1,2, a)} Lukas Liensberger,^{1,2} Matthias Althammer,^{1,2} Hans Huebl,^{1,2,3,4} Stephan Geprägs,¹ Katrin Schultheiss,⁵ Aleksandr Buzdakov,⁵ Tobias Hula,⁵ Helmut Schultheiss,⁵ Eric R. J. Edwards,⁶ Hans T. Nembach,⁶ Justin M. Shaw,⁶ Rudolf Gross,^{1,2,3,4} and Mathias Weiler^{1,2, b)}

¹⁾ *Walther-Meißner Institute, Bayerische Akademie der Wissenschaften, 85748 Garching, Germany*

²⁾ *Physics Department, Technical University of Munich, 85748 Garching, Germany*

³⁾ *Nanosystems Initiative Munich, 80799 Munich, Germany*

⁴⁾ *Munich Center for Quantum Science and Technology (MCQST), 80799 Munich, Germany*

⁵⁾ *Helmholtz-Zentrum Dresden-Rossendorf, 01328 Dresden, Germany*

⁶⁾ *Quantum Electromagnetics Division, National Institute of Standards and Technology, Boulder, CO 80305, USA*

(Dated: 30 August 2019)

I. SATURATION MAGNETIZATION

In order to extract the saturation magnetization of our CoFe samples, we measured the effective magnetization M_{eff} and plotted those values vs. the inverse FM thickness (see Fig. S1). The y-intercept of a linear fit to the data returns $\mu_0 M_s = (2.35 \pm 0.02)$ T. This method was shown to result in good agreement with SQUID magnetometry measurements in Schoen's *et al* work¹.

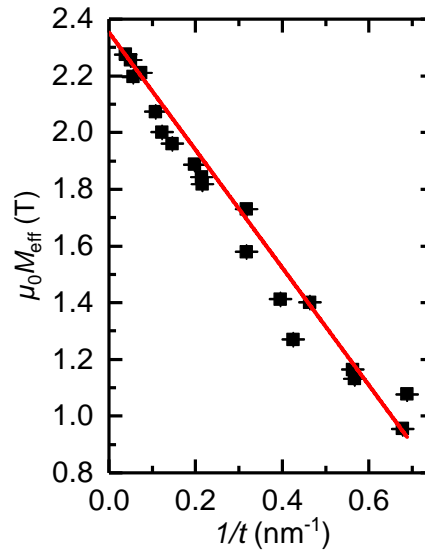


FIG. S1. Effective magnetization vs. reciprocal thickness t of the samples. The extrapolated bulk value returns the saturation magnetization $\mu_0 M_s = 2.35$ T.

^{a)} Electronic mail: luis.flacke@wmi.badw.de

^{b)} Electronic mail: mathias.weiler@wmi.badw.de

II. LINEWIDTH ANALYSIS

The total linewidth of the resonance comprises several contributions, coming from different damping processes and long range order inhomogeneities. The total damping $\alpha_G = \alpha_0 + \alpha_{sp} + \alpha_{eddy} + \alpha_{rad}$ can be translated to different contributions to the linewidth given as

$$\mu_0 \Delta H = \mu_0 H_{inh} + 2 \cdot \frac{2\pi f \alpha_G}{\gamma}, \quad (S1)$$

which is demonstrated for the $t = 26$ nm sample in FigS2. From the total linewidth we extract α_G for the samples as shown in Fig. 2 (b). The radiative damping and eddy current contributions to the Gilbert damping parameter are quantified and calculated back to a corresponding linewidth contribution, with help of the second summand of Eq. (S1). In order to get an intuition of the influence of each contribution we subtract them one by one from the total damping. To exemplify the vanishing influence of eddy currents in our samples, we start by subtracted this component ($\alpha_{eddy} \approx 8.5 \times 10^{-5}$) with remaining linewidth shown as yellow circles. The next two steps are subtracting the radiative damping ($\alpha_{rad} = (4.69 \pm 0.09) \times 10^{-4}$) and the inhomogeneous linewidth broadening ($\mu_0 \Delta H = (1.00 \pm 0.06)$ mT). The remaining linewidth comes from the intrinsic damping and spin pumping to the adjacent layers. The latter effect is quantified with Fig2 (b) as $\alpha_{sp} = (3.45 \pm 0.57) \times 10^{-4}$ and its contribution to the linewidth was then also subtracted. The slope of the resulting ΔH vs. f then allows to determine the intrinsic damping of $\alpha_0 = (3.18 \pm 0.48) \times 10^{-4}$ for this sample.

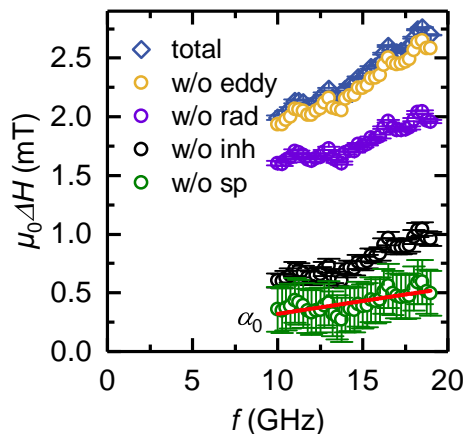


FIG. S2. Linewidth vs. frequency for a Ta(3 nm)/Al(3 nm)/Co₂₅Fe₇₅(26 nm)/Al(3 nm)/Ta(3 nm) sample measured by OOP BB-FMR. The blue diamonds show the total measured linewidths, whereas yellow, purple, black and green circles were obtained by subtracting different contributions one by one, namely, eddy currents, radiative damping, inhomogeneous linewidth broadening, and spin pumping, respectively.

III. IN PLANE BB-FMR DATA FOR SPIN-WAVE PROPAGATION

Together with the structured sample B (Pt(3 nm)/Cu(3 nm)/Co₂₅Fe₇₅(26 nm)/Cu(3 nm)/Ta(3 nm)) we co-deposited blanket films. With these reference samples, we performed in-plane BB-FMR in order to extract the necessary magnetic properties of the structured films to simulate the spin-wave propagation length and dispersion as shown in Fig. 3 (f) and (g). From the resonance field $\mu_0 H_{\text{res}}$ vs. f (see Fig. S3), we obtain the Landé-factor g and $\mu_0 M_{\text{eff}}$ by using the in-plane Kittel formula:

$$\mu_0 H_{\text{res}} = \sqrt{\left(\frac{fh}{g\mu_B}\right)^2 + \left(\frac{\mu_0 M_{\text{eff}}}{2}\right)^2} - \frac{\mu_0 M_{\text{eff}}}{2} - \mu_0 H_{\text{aniIP}}. \quad (\text{S2})$$

Here, h is the Planck constant, μ_B is the Bohr magneton, and H_{aniIP} is the growth dependent in-plane anisotropy field, which is negligible in our samples. The difference between $\mu_0 M_s$ and $\mu_0 M_{\text{eff}}$ returns the effective out-of-plane anisotropy field $\mu_0 H_k$. From the slope of the linewidth $\mu_0 \Delta H$ vs. f , we obtain the damping parameter α_G . The radiative damping is subtracted as this contribution is not present in our spin-wave propagation experiment. As the BLS measurements was performed in a small frequency range, we only took the low-frequency part ($f < 15$ GHz) for the determination of $\alpha_G - \alpha_{\text{rad}}$. Note that the slight deviation from linear ΔH vs. f behavior observed in Fig. S3 (b) is indicative of two-magnon scattering, as expected in the in-plane configuration.

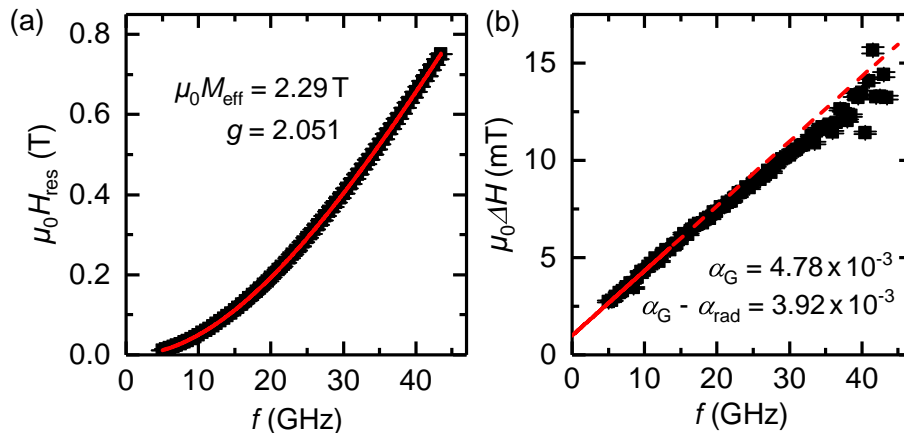


FIG. S3. (a) Resonance field vs. frequency. The red curve is a fit to Eq. (S2). (b) Linewidth vs. frequency. The Gilbert damping parameter was extracted from the same frequency range, where we also performed the spin-wave propagation experiments. In order to determine the effective damping for our spin waves in the BLS measurement we subtracted the radiative damping contribution which is only present in our BB-FMR setup and not in the patterned devices.

¹M. A. W. Schoen, D. Thonig, M. L. Schneider, T. J. Silva, H. T. Nembach, O. Eriksson, O. Karis, and J. M. Shaw, Nature Physics **12**, 839 (2016)